Protein-Level Fluctuation Correlation at the Microcolony Level and Its Application to the *Vibrio harveyi* Quorum-Sensing Circuit

Yufang Wang,[†] Kimberly C. Tu,[‡] N. P. Ong,[†] Bonnie L. Bassler,[‡§] and Ned S. Wingreen[‡]

[†]Department of Physics, [‡]Department of Molecular Biology, and [§]Howard Hughes Medical Institute, Princeton University, Princeton, New Jersey

S1 Materials and Methods

S1.1 *Vibrio harveyi* strains

All *Vibrio harveyi* strains are derived from wild-type BB120 (1). *V. harveyi* deletions and mutations were constructed using previously described methods (2), and all fluorescent constructs were introduced onto the chromosome of a *V. harveyi* Δ*luxM*, Δ*luxS*, Δ*cqsS* strain by allelic replacement (3). As a result, these strains are not able to synthesize but remain responsive to two autoinducers (AIs), HAI-1 and AI-2. These strains have no receptor for the third AI, CAI-1.

An N-terminal YFP-LuxO construct was engineered by overlapping PCR to generate a $(Gly_4Ser)_3$ linker between the two proteins, and this construct was subsequently cloned into the EcoRI and BamHI sites in pFED342 (pKT1416). The YFP plasmid pDH6-YFP was a generous gift from Michael Elowitz (California Institute of Technology). A 3-kB fragment containing the *V. harveyi luxO* region was cloned into the EcoRI and BamHI sites in pFED342 to generate pKT1322. A Cm resistance gene was recombined downstream of the *qrr*1 gene to generate pKT1365. Site-directed mutagenesis was performed to engineer a mutation that disrupts LuxO auto-repression (*luxO*-ar, pKT1385). Overlapping PCR was used to recombine mutations into pBB147 (3) to generate pKT1445 (WT) and pKT1449 (*luxO*-ar). These cosmids were subsequently conjugated into *V. harveyi* and genes introduced onto the chromosome. The drug resistance markers were removed by homologous recombination by conjugating with pTL18 (4).

The *qrr*4-*cfp* transcriptional fusion was generated by PCR from pDH3-CFP plasmid (also from Michael Elowitz), and the construct was subsequently recombined into cosmid 28-13 which contains the *V. harveyi qrr*4 genomic region to generate pKT1486.

The mCherry plasmid pRSET-B was a generous gift from Roger Tsien (University of California at San Diego) (5). An N-terminal mCherry-LuxR construct was engineered by overlapping PCR to generate a $(Gly_4Ser)_3$ linker between the two proteins. This construct was subsequently cloned into the EcoRI and BamHI sites in pFED342 (pKT1412). A Kan^R marker was cloned in the downstream BamHI site (pKT1438), and this plasmid was used as the PCR template to generate a linear DNA product with homologous ends to recombine into the native *luxR* locus in pBB1805 to generate KT1630, which was subsequently conjugated into *V. harveyi* (6).

The final strains KT651 (wt) and KT653 (*luxO*-ar) used in this study both have three fluorescent protein fusions: YFP-LuxO replacing the native LuxO, mCherry-LuxR replacing the native LuxR, and *qrr*4-*cfp* is used to report the activity of the *qrr*4 promoter.

Studies of protein stability in *E. coli* reveal that the majority of protein species that are synthesized in *E. coli* are stable, and the turnover rate of those proteins is extremely slow (7). GFP expressed in *E. coli* is stable with a half life of more than 1 day. To make GFP susceptible to the action of indigenous housekeeping proteases, short peptide sequences need to be added to the C-terminal of GFP (8). Based on the similarity between fluorescent proteins and between *V. harveyi* and *E. coli*, we assume the fluorescent proteins used in this study are stable in *V. harveyi*. As there is no previous report of degradation of

V. harveyi LuxO and LuxR, it is very likely that the fluorescent protein fusions YFP-LuxO and mCherry-LuxR are stable proteins in *V. harveyi*.

S1.2 Time-lapse microscopy and image analysis

Cells were grown in AB medium (10 mM $K_xH_yPO_4$, 300 mM NaCl, 50 mM $MgSO_4$, 0.2% vitamin-free casamino acids, 10 mM L-arginine, 1% glycerol, pH 7.5) supplied with equal amounts of HAI-1 and AI-2 at 0 nM (low AI concentration), 50 nM (intermediate AI concentration) and 1 μM (high AI concentration). The culture was grown to OD $\sim$ 0.5 at 30°C. An aliquot of culture was pipetted onto a glass coverslip and covered with a 1% agarose pad. The agarose pads were pre-soaked overnight in the identical medium in which the cells were grown. A second piece of coverslip was placed on top of the agarose pad to prevent water evaporation. Mineral oil was used to seal the agarose pad between the two coverslips. Multiple sets of these agarose pads were arranged on a single coverslip so that different strains could be monitored simultaneously.

Growth of microcolonies was monitored by light microscopy at room temperature using a Nikon TE2000-U microscope equipped with ProScanII microscope automation system (Prior Scientific, Rockland, MA) and a CFP/YFP/mCherry fluorescence filter set (89006, Chroma Technology Corp, Bellows Falls, VT). To control the microscope and the EMCCD camera (DV877-DCS-BV, Andor Technology, South Windsor, CT), custom scripts were written in Andor Basic. Images were acquired in multiple fluorescent channels as well as in the transmitted white light channel at 10-minute intervals.

Fluorescence analysis of cell lineages was done with custom MATLAB software, which has three stages: first, images are segmented to select all individual microcolonies or cells; next, microcolonies or cells are tracked between frames to establish the cell lineage tree; and, finally, fluorescence intensities for each microcolony or cell lineage are compiled. Each step is manually checked and corrected extensively. The mean doubling time, which defines the time unit "generation", was measured by fitting the total area of all the microcolonies to a single exponential function of time.

We found that *V. harveyi*'s autofluorescence changes over time after the cells are transferred from liquid culture to under an agarose pad. A control wt *V. harveyi* strain without any fluorescent label (BB120) was imaged to establish the autofluorescence baseline. The mean autofluorescence of BB120 at time t after transfer was then subtracted from the measured fluorescence signal also at time t after transfer.

S1.3 Correlation calculation from experimental data

To calculate fluctuation correlation, we define $X_i(t)$ and $Y_i(t)$ to represent any two protein concentrations at time t, and i is used to index the microcolony or single-cell. We define $x_i(t)$ and $y_i(t)$ to be any of the concentration deviations from the expected values. The

expected values and the concentration deviations (fluctuations) are expressed by

$$\langle X(t)\rangle = \frac{1}{N}\sum_{i=1}^{N} X_i(t), \quad x_i(t) = X_i(t) - \langle X(t)\rangle. \tag{S1}$$

The correlation S and normalized correlation R between the fluctuations x and y is given by

$$S_{x,y}(t_1,t_2) = \frac{1}{N}\sum_{i=1}^{N} x_i(t_1)y_i(t_2), \tag{S2}$$

$$R_{x,y}(t_1,t_2) = \frac{S_{x,y}(t_1,t_2)}{\sqrt{S_{x,x}(t_1,t_1)S_{y,y}(t_2,t_2)}}, \tag{S3}$$

The correlation matrix $R_{x,y}(t_1,t_2)$ defined in Eq. S3 plays a major role in our subsequent analysis. The time coordinates (t_1,t_2) serve as the indices specifying a matrix element of $R_{x,y}(t_1,t_2)$.

In principle $S_{x,x}(t,t)$ is the same as true signal standard deviation squared $\sigma_x^2(t)$. In experiment when $x_i(t)$ is measured there is a random imaging noise $\xi_i^x(t)$ included in the measurement, with $\langle \xi_i^x(t_1)\xi_j^y(t_2)\rangle \approx v_i^x\delta_{xy}\delta_{ij}\delta(t_1-t_2)$. As a result,

$$S_{x,y}^{\mathrm{raw}}(t_1,t_2) \approx \frac{1}{N}\sum_{i=1}^{N} x_i(t_1)y_i(t_2) + \delta_{xy}\delta(t_1-t_2)\sum_{i=1}^{N} v_i^x. \tag{S4}$$

Therefore it is not accurate to use $S_{x,x}^{\mathrm{raw}}(t,t)$ to normalize correlation. Rather we extrapolate $S_{x,x}^{\mathrm{correct}}(t,t)$ from the neighboring elements in the raw autocorrelation matrix

$$S_{x,x}^{\mathrm{correct}}(t,t) = S_{x,x}^{\mathrm{raw}}(t-dt,t) + S_{x,x}^{\mathrm{raw}}(t,t-dt) - S_{x,x}^{\mathrm{raw}}(t-dt,t-dt), \tag{S5}$$

where dt is the time interval between two consecutive image frames. The correlation matrixes are then normalized as indicated in Eq. S3 using $S_{x,x}^{\mathrm{correct}}(t_1,t_1)$ and $S_{y,y}^{\mathrm{correct}}(t_2,t_2)$.

Ideally, when the regulation process is time-invariant, the two-dimensional correlation heat map $R_{x,y}(t_1,t_2)$ can be reduced to a one-dimensional correlation curve

$$R_{x,y}(\tau) = \langle R_{x,y}(t_1,t_2)\rangle|_{t_1-t_2=\tau}. \tag{S6}$$

However, when the correlation matrix is constructed from experimental data, deviations from this simple pattern indicate that the regulation parameters have changed over the course of the experiment. Our experiments were designed to minimize such changes. Data sets in which large regions of the correlation heat map display horizontal or vertical swaths with nominally uniform values might be caused by individual cells that failed to follow the population behavior. Such individual cells and their associated microcolonies were carefully excluded from the analysis.

S2 Analytical solutions of correlation functions

We consider the same model system as in (9). In this model system, a protein A regulates the production of mRNA for protein B. The equilibrium concentration relationship between A and B is shown in Fig. S1 *a*. The equations for the protein concentrations A, B and their corresponding mRNAs concentrations m_A and m_B are

$$\begin{aligned} \dot{m}_A &= \alpha_{mA} - \kappa m_A + \eta_{mA} + \theta_{mA} E, && \text{(S7)} \\ \dot{A} &= \alpha_A m_A - \beta A + \eta_A + \theta_A E, && \text{(S8)} \\ \dot{m}_B &= Q(A) - \kappa m_B + \eta_{mB} + \theta_{mB} E, && \text{(S9)} \\ \dot{B} &= \alpha_B m_B - \beta B + \eta_B + \theta_B E. && \text{(S10)} \end{aligned}$$

E represents extrinsic noise whose source is modeled as an Ornstein-Uhlenbeck process

$$\dot{E} = -\beta E + \eta_{\mathrm{E}}. \quad \text{(S11)}$$

We assume the noise terms η_i for $i = \{mA, A, mB, B, E\}$ are independent, delta-correlated in time (white), similarly distributed processes that arise from the stochastic nature of chemical reactions at the single molecule level, $\langle \eta_i(t_1)\eta_j(t_2)\rangle = W_i \delta_{ij}\delta(t_1 - t_2)$. Assuming no protein degradation, β is the dilution rate due to cell volume growth. For a cell that doubles its volume every cell cycle, $\beta = \log 2$ generation^{-1}. The parameter κ defines the total dilution and degradation rate of mRNA molecules. Usually mRNA has a high degradation rate, $\kappa \gg \beta$. The degree that a protein is affected by extrinsic noise is set by θ_i. $Q(A)$ is a Hill function such that $Q(A) = \frac{\alpha_B}{1+(K/A)^h}$, where K is a dissociation constant and h is either the Hill coefficient (for $h > 0$, meaning A positively regulates B) or the negative Hill coefficient (for $h < 0$, meaning A negatively regulates B). In the case of $h = 0$, A does not regulate B.

The noise sources have zero mean so the equilibrium point of the deterministic system can be calculated as $m_{Aeq} = \frac{\alpha_{mA}}{\kappa}, A_{eq} = \frac{\alpha_A \alpha_{mA}}{\kappa\beta}, m_{Beq} = \frac{Q(A_{eq})}{\kappa}$, and $B_{eq} = \frac{\alpha_B Q(A_{eq})}{\kappa\beta}$. We expect perturbations due to noise to be small, so it is valid to linearize the system about the equilibrium point. Defining $m_a = m_A - m_{Aeq}, a = A - A_{eq}, m_b = m_B - m_{Beq}$ and $b = B - B_{eq}$. We obtain the following set of linear kinetic equations

$$\begin{aligned} \dot{m}_a &= -\kappa m_a + \eta_{mA} + \theta_{mA} E, && \text{(S12)} \\ \dot{a} &= \alpha_A m_a - \beta a + \eta_A + \theta_A E, && \text{(S13)} \\ \dot{m}_b &= q a - \kappa m_b + \eta_{mB} + \theta_{mB} E, && \text{(S14)} \\ \dot{b} &= \alpha_B m_b - \beta b + \eta_B + \theta_B E, && \text{(S15)} \end{aligned}$$

where q is the local sensitivity, $q = \frac{dQ(A)}{dA}|_{A=A_{eq}}$. $q > 0$ means positive regulation and $q < 0$ means negative regulation of B by A. (At either very high or very low A_{eq} where the $Q(A)$ vs. A curve flattens out, q is close to zero, meaning that regulation is inactive.)

In order to calculate the correlation of two time series, it is convenient to use Fourier

transforms and to perform the operation in the frequency domain. The correlation of two time series $f(t)$ and $g(t)$ in the time domain is equivalent to multiplication in the frequency domain. We have for the convolution

$$S_{f,g}(\tau) = \int_{-\infty}^{+\infty} f(t)g(t+\tau)dt = F^{-1}[\tilde{f}^*(\omega)\tilde{g}(\omega)], \tag{S16}$$

where $\tilde{f}(\omega)$ and $\tilde{g}(\omega)$ are, respectively, the Fourier transforms of $f(t)$ and $g(t)$, and F^{-1} represents the inverse Fourier transform.

Taking the Fourier transform of Eqs. S11-S15, we find

$$\begin{aligned}
\tilde{m}_a &= \frac{1}{i\omega+\kappa}(\tilde{\eta}_{mA} + \theta_{mA}\tilde{E}), && \text{(S17)}\\
\tilde{a} &= \frac{1}{i\omega+\beta}(\alpha_A\tilde{m}_a + \tilde{\eta}_A + \theta_A\tilde{E}), && \text{(S18)}\\
\tilde{m}_b &= \frac{1}{i\omega+\kappa}(q\tilde{a} + \tilde{\eta}_{mB} + \theta_{mB}\tilde{E}), && \text{(S19)}\\
\tilde{b} &= \frac{1}{i\omega+\beta}(\alpha_B\tilde{m}_b + \tilde{\eta}_B + \theta_B, \tilde{E}) && \text{(S20)}\\
\tilde{E} &= \frac{1}{i\omega+\beta}\tilde{\eta}_E. && \text{(S21)}
\end{aligned}$$

The correlations can be calculated using Fourier transform and Cauchy's Residue Theorem. The white noise terms η_i have a constant power spectral density, viz. $\langle\tilde{\eta}_i^*(\omega)\tilde{\eta}_i(\omega)\rangle = W_i$, $i = \{mA, A, mB, B, E\}$. Moreover, the noise terms for different reactions are assumed to be uncorrelated, i.e. $\langle\eta_i(t+\tau)\eta_j(t)\rangle_t = 0$ for $i \neq j$, thus $\langle\tilde{\eta}_i^*(\omega)\tilde{\eta}_j(\omega)\rangle = 0$ for $i \neq j$. These features simplify calculations of the cross- and autocorrelations.

Our model becomes the same as that in (9) if we assume the following: first, mRNA production is not affected by extrinsic noise, $\theta_{mA} = \theta_{mB} = 0$, second, protein intrinsic noise mainly comes from mRNA noise not from protein synthesizing itself, $W_A = W_B = 0$ or $\eta_A = 0$ and $\eta_B = 0$, third, protein A and B are equally affected by extrinsic noise $\theta_A = \theta_B$. However, these three assumptions cannot always be justified in general. Nevertheless, if all the parameters are kept, the analytical results become very complicated. Therefore, below we simplify the system in a way that preserves most kinetic properties but is also intuitive.

S2.1 Should mRNA kinetics always be kept?

In this section we will discuss if we can simplify the system by assuming mRNA always reach equilibrium fast, therefore we do not need to consider the mRNA kinetics at the timescale of $1/\kappa$.

For the unregulated protein A, assuming no extrinsic noise, $\theta_{mA} = 0$ and $\theta_A = 0$. From

Eqs. S12, S13, S17, and S18, without E terms, we have

$$\begin{aligned} S_{m_a,m_a}(\tau) &= \int_{-\infty}^{+\infty} m_a(t+\tau)m_a(t)dt \\ &= F^{-1}(\frac{W_{mA}}{\omega^2+\kappa^2}) \\ &= \frac{W_{mA}}{2\kappa}e^{-\kappa|\tau|}, \end{aligned} \tag{S22}$$

$$\begin{aligned} S_{a,a}(\tau) &= \int_{-\infty}^{+\infty} a(t+\tau)a(t)dt \\ &= F^{-1}(\frac{W_A}{\omega^2+\beta^2}+\frac{\alpha_A^2 W_{mA}}{(\omega^2+\kappa^2)(\omega^2+\beta^2)}) \\ &= \frac{W_A}{2\beta}e^{-\beta|\tau|}+\frac{\alpha_A^2 W_{mA}}{2(\kappa^2-\beta^2)}(\frac{e^{-\beta|\tau|}}{\beta}-\frac{e^{-\kappa|\tau|}}{\kappa}). \end{aligned} \tag{S23}$$

The kinetic process described in Eq. S7 without the E term produces a Poisson distribution for m_A molecules per unit volume. Hence the squared standard deviation σ^2 equals mean $\langle N\rangle$,

$$\langle N_{mA}\rangle = V\cdot m_{Aeq} = \frac{V\alpha_{mA}}{\kappa}, \tag{S24}$$

$$\sigma_{mA}^2 = V^2\cdot S_{m_a,m_a}(0) = \frac{V^2 W_{mA}}{2\kappa} = \langle N_{mA}\rangle, \tag{S25}$$

yielding

$$W_{mA} = \frac{2\alpha_{mA}}{V}. \tag{S26}$$

Similarly, if there is no noise in the m_A level ($W_{mA}=0$), Eq. S8 without the E term also produces a Poisson distribution of A molecules per unit volume,

$$\langle N_A\rangle|_{W_{mA}=0} = V\cdot A_{eq} = \frac{V\alpha_A m_A}{\beta}, \tag{S27}$$

$$\sigma_A^2|_{W_{mA}=0} = V^2\cdot S_{a,a}(0)|_{W_{mA}=0} = \frac{V^2 W_A}{2\beta} = \langle N_A\rangle|_{W_{mA}=0}, \tag{S28}$$

$$W_A = \frac{2\alpha_A m_A}{V}. \tag{S29}$$

Including both the intrinsic noises from synthesizing mRNA and from synthesizing protein molecules, the mean protein molecule number $\langle N_A\rangle$ does not change, but the standard

deviation becomes larger

$$\begin{aligned}\sigma_A^2 &= V^2 \cdot S_{a,a}(0) \\ &= \frac{V^2 W_A}{2\beta} + \frac{V^2 \alpha_A^2 W_{mA}}{2\kappa\beta(\kappa+\beta)} \\ &= V A_{eq}(1 + \frac{\alpha_A}{\beta+\kappa}). \end{aligned} \tag{S30}$$

In the limit of $\kappa \gg \beta$ (10, 11), $\frac{\alpha_A}{\beta+\kappa} \approx \frac{\alpha_A}{\kappa} = b_A$ is the burst size, i.e., the average number of molecules made from a single copy of mRNA before it is degraded. With $\langle N_A \rangle = V A_{eq}$, we have $\sigma_A^2 \approx \langle N_A \rangle (1 + b_A)$, which agrees with previous report (12). b was measured to be around 20 for the repressed *E. coli lacZ* gene (13). The autocorrelation of A fluctuation is then

$$\begin{aligned} S_{a,a}(\tau) &\approx \frac{A_{eq}}{V}[e^{-\beta|\tau|} + b\frac{\kappa\beta}{\kappa-\beta}(\frac{e^{-\beta|\tau|}}{\beta} - \frac{e^{-\kappa|\tau|}}{\kappa})] \\ &\approx \frac{A_{eq}}{V}[(1+b)e^{-\beta|\tau|} + \frac{b\beta}{\kappa}e^{-\kappa|\tau|}] \end{aligned} \tag{S31}$$

On the other hand if one assumes mRNA always reach equilibrium fast, one can formally write

$$\dot{m}_A = \alpha_{mA} - \kappa m_A + \eta_{mA} + \theta_{mA} E = 0, \tag{S32}$$

$$m_A = \frac{1}{\kappa}(\alpha_{mA} + \eta_{mA} + \theta_{mA} E). \tag{S33}$$

Insert this the expression for m_A into Eq. S8 yields

$$\dot{A} = \alpha_{mA} b_A - \beta A + (\eta_A + b_A \eta_{mA}) + (\theta_A + b_A \theta_{mA}) E. \tag{S34}$$

Note that the form is the same as Eq. S7, only the noise strength and time constants are different. For this simplified form, in the case of no extrinsic noise,

$$\begin{aligned} S'_{a,a}(\tau) &= \frac{W_A}{2\beta}e^{-\beta|\tau|} + (\frac{\alpha_A}{\kappa})^2 \frac{W_{mA}}{2\beta}e^{-\beta|\tau|} \\ &\approx \frac{A_{eq}}{V}(1+b_A)e^{-\beta|\tau|} \end{aligned} \tag{S35}$$

The fractional difference in protein noise due to mRNA kinetics is then

$$\frac{S_{a,a}(\tau) - S'_{a,a}(\tau)}{S'_{a,a}(\tau)} = \frac{b\beta e^{\beta|\tau|}}{(1+b)\kappa e^{\kappa|\tau|}}, \tag{S36}$$

which decreases with increasing $|\tau|$. The maximum fractional difference is $\frac{b\beta}{(1+b)\kappa}$ at $\tau = 0$. Thus, if $\kappa \gg \beta$, i.e., the mRNA turn over rate is much faster than that of protein, it is

accurate to assume that mRNA always reaches equilibrium fast. Eqs. S7-S10 can then be simplified as

$$\dot{A} = \alpha'_A - \beta A + \eta'_A + \theta'_A E, \tag{S37}$$
$$\dot{B} = Q'(A) - \beta B + \eta'_B + \theta'_B E, \tag{S38}$$

where $\alpha'_A = \alpha_{mA} b_A$, $\eta'_A = \eta_A + b_A \eta_{mA}$, $\theta'_A = \theta_A + b_A \theta_{mA}$, $Q'(A) = b_B Q(A)$, $\eta'_B = \eta_B + b_B \eta_{mB}$, and $\theta'_B = \theta_B + b_B \theta_{mB}$. We also have $W'_A = 2\beta A_{eq}(1 + b_A)/V$ and $W'_B = 2\beta B_{eq}(1 + b_B)/V$.

S2.2 One protein regulating another

If we linearize Eqs. S37-S38 about equilibrium we have

$$\dot{a} = -\beta a + \eta'_A + \theta'_A E, \tag{S39}$$
$$\dot{b} = q' a - \beta b + \eta'_B + \theta'_B E. \tag{S40}$$

Then, taking the Fourier transform gives

$$\tilde{a} = \frac{\tilde{\eta}'_A}{i\omega + \beta} + \frac{\theta'_A \tilde{\eta}_E}{(i\omega + \beta)^2}, \tag{S41}$$
$$\tilde{b} = \frac{\tilde{\eta}'_B}{i\omega + \beta} + \frac{\theta'_B \tilde{\eta}_E + q' \tilde{\eta}'_A}{(i\omega + \beta)^2} + \frac{q' \tilde{\theta}'_A \tilde{\eta}_E}{(i\omega + \beta)^3}. \tag{S42}$$

The correlations can be calculated as

$$\begin{aligned}
S_{a,a}(\tau) &= \int_{-\infty}^{+\infty} a(t+\tau)a(t)dt \\
&= F^{-1}(\frac{W'_A}{\omega^2+\beta^2} + \frac{\theta'^2_A W_E}{(\omega^2+\beta^2)^2}) \\
&= \frac{W'_A}{2\beta}e^{-\beta|\tau|} + \frac{\theta'^2_A W_E}{4\beta^3}e^{-\beta|\tau|}(1+\beta|\tau|), \qquad \text{(S43)} \\
S_{b,b}(\tau) &= \int_{-\infty}^{+\infty} b(t+\tau)b(t)dt \\
&= F^{-1}(\frac{W'_B}{\omega^2+\beta^2} + \frac{\theta'^2_B W_E + q'^2 W'_A}{(\omega^2+\beta^2)^2} + \frac{q'^2\theta'^2_A W_E}{(\omega^2+\beta^2)^3}) \\
&= \frac{W'_B}{2\beta}e^{-\beta|\tau|} + \frac{\theta'^2_B W_E + q'^2 W'_A}{4\beta^3}e^{-\beta|\tau|}(1+\beta|\tau|) + \\
&\quad \frac{q'^2\theta'^2_A W_E}{16\beta^5}e^{-\beta|\tau|}(3+3\beta|\tau|+\beta^2\tau^2), \qquad \text{(S44)} \\
S_{a,b}(\tau) &= \int_{-\infty}^{+\infty} a(t+\tau)b(t)dt \\
&= F^{-1}(\frac{\theta'_A\theta'_B W_E}{(\omega^2+\beta^2)^2} + \frac{q' W'_A}{(\omega^2+\beta^2)(-i\omega+\beta)} + \frac{q'\theta'^2_A W_E}{(\omega^2+\beta^2)^2(-i\omega+\beta)}) \\
&= \frac{\theta'_A\theta'_B W_E}{4\beta^3}e^{-\beta|\tau|}(1+\beta|\tau|) + \\
&\quad \begin{cases} \frac{q'W'_A}{4\beta^2}e^{\beta\tau}(1-2\beta\tau) + \frac{q'\theta'^2_A W_E}{16\beta^4}e^{\beta\tau}(2\beta^2\tau^2-4\beta\tau+3) & \text{if } \tau<0 \\ \frac{q'W'_A}{4\beta^2}e^{-\beta\tau} + \frac{q'\theta'^2_A W_E}{16\beta^4}e^{-\beta\tau}(2\beta\tau+3) & \text{if } \tau\geq 0 \end{cases}. \qquad \text{(S45)}
\end{aligned}$$

The correlations are further normalized to

$$R_{f,g}(\tau) = \frac{S_{f,g}(\tau)}{\sqrt{S_{f,f}(0)S_{g,g}(0)}}. \qquad \text{(S46)}$$

In the limit of low extrinsic noise ($W_E = 0$) we have

$$\begin{aligned}
R_{a,a}(\tau)|_{W_E=0} &= e^{-\beta|\tau|}, \qquad \text{(S47)} \\
R_{b,b}(\tau)|_{W_E=0} &= n_1 e^{-\beta|\tau|} + n_2 e^{-\beta|\tau|}(1+\beta|\tau|), \qquad \text{(S48)} \\
R_{a,b}(\tau)|_{W_E=0} &= \begin{cases} n_3 e^{\beta\tau}(1-2\beta\tau) & \text{if } \tau<0 \\ n_3 e^{-\beta\tau} & \text{if } \tau\geq 0 \end{cases}. \qquad \text{(S49)}
\end{aligned}$$

where the normalization factors are

$$n_1 = \frac{2\beta^2 W'_B}{2\beta^2 W'_B + q'^2 W'_A} \tag{S50}$$

$$n_2 = \frac{q'^2 W'_A}{2\beta^2 W'_B + q'^2 W'_A} \tag{S51}$$

$$n_3 = \frac{q' W'_A}{\sqrt{2W'_A(2\beta^2 W'_B + q'^2 W'_A)}} \tag{S52}$$

In this case the autocorrelation of A fluctuations $R_{a,a}(\tau)|_{W_E=0}$ has a sharp peak at $\tau = 0$ as $\frac{dR_{a,a}(\tau)}{d\tau}|_{\tau=0-\epsilon} > 0$ while $\frac{dR_{a,a}(\tau)}{d\tau}|_{\tau=0+\epsilon} < 0$ ($\epsilon \ll 1$). The full width at half maximum (FWHM) is $\frac{2\log 2}{\beta} = 2$ generations. The autocorrelation of B fluctuations $R_{b,b}(\tau)|_{W_E=0}$ is wider than that of A regardless whether the regulation is positive or negative. Its peak width depends on how much of the fluctuation of B comes from its upstream regulator A. The maximum FWHM of ~ 4.8 generations can be reached if B fluctuations are dominated by that propagated from A. In this limit, $R_{b,b} = (1 + |\tau|)e^{-\beta|\tau|}$, the autocorrelation peak top is rounded as $\frac{dR_{b,b}(\tau)}{d\tau}|_{\tau=0} = 0$. The cross-correlation between A and B fluctuations $R_{a,b}(\tau)|_{W_E=0}$ has an extreme value at $\tau = -\frac{1}{2\beta} \simeq -0.72$ generation (Fig. S1 *d*). The maximum possible absolute cross-correlation is $\sqrt{2}e^{-\frac{1}{2}} \simeq 0.86$ when $W'_B = 0$ and $\tau = -\frac{1}{2\beta}$.

When $W_E > 0$ but $\theta'_A = 0$, meaning that upstream regulator has no extrinsic noise, we get $R_{a,b}(\tau)|_{\theta'_A=0} \propto R_{a,b}(\tau)|_{W_E=0}$. The time lag that maximizes the normalized correlation amplitude does not change for $\theta'_A = 0$ vs. $W_E = 0$, but the amplitude is lower for $\theta'_A = 0$ than $W_E = 0$.

If $W_E > 0$, $\theta'_A > 0$ and $\theta'_B > 0$, then because the time scale of extrinsic noise ($1/\beta$) is slower than that of intrinsic noise ($1/\kappa$ for mRNA kinetics and 0 for synthesizing protein itself), the autocorrelation peaks of A and B fluctuations each becomes wider than without extrinsic noise. The maximum FWHM of A fluctuation autocorrelation $R_{a,a}(\tau)$ reaches ~ 4.8 generations if noise in A is dominated by extrinsic noise. The maximum FWHM of B fluctuation autocorrelation $R_{b,b}(\tau)$ reaches ~ 6.7 generations if $W'_B = 0$, $\theta'_B = 0$, and $\theta'_A \gg \beta$. With $\theta'_A \gg \beta$ the extreme peak of $R_{a,b}(\tau)$ shifts from $\tau = -\frac{1}{2\beta} \simeq -0.72$ generation to $\tau = -\frac{1}{\sqrt{2}\beta} \simeq -1.02$ generation. In the case that A and B are both directly affected by extrinsic noise ($\theta'_A > 0, \theta'_B > 0$), the cross-correlation $R_{a,b}(\tau)$ has a symmetric part about $\tau = 0$. For positive regulation, it shifts the $|R_{a,b}(\tau)|$ peak towards $\tau = 0$. For negative regulation, it shifts the $|R_{a,b}(\tau)|$ peak away from $\tau = 0$.

S2.3 Autocorrelation for a protein that regulates itself

Now consider a protein P that regulates its own gene expression. The equations for the protein concentrations P and its mRNA concentration m_P are

$$\dot{m}_P = Q(P) - \kappa m_P + \eta_{mP} + \theta_{mP} E, \tag{S53}$$

$$\dot{P} = \alpha_P m_P - \beta P + \eta_P + \theta_P E, \tag{S54}$$

where we let $Q(P) = \alpha_P/[1+(K/P)^h]$. Again, assuming mRNA always reaches equilibrium

$$\begin{aligned} m_P &= \frac{1}{\kappa}[Q(p) + \eta_{mP} + \theta_{mP}E], && \text{(S55)} \\ \dot{P} &= b_P Q(P) - \beta P + (\eta_P + b_P\eta_{mP}) + (\theta_P + b_P\theta_{mP})E, && \text{(S56)} \end{aligned}$$

where $b_P = \alpha_P/\kappa$. The deterministic equilibrium of Eq. S56 is set by $b_P Q(P_{eq}) = \beta P_{eq}$ as shown in Fig. S1 *e*. Defining $p = P - P_{eq}$, and linearizing Eq. S56 about P_{eq} yields

$$\dot{p} = -(\beta - \gamma)p + \eta'_P + \theta'_P E. \qquad \text{(S57)}$$

where $\gamma = b_P \frac{dQ(P)}{dP}|_{P=P_{eq}}$. $\gamma > 0$ means positive feedback and $\gamma < 0$ means negative feedback or auto-repression. Note that the linearization is only valid for $\gamma < \beta$, for $\gamma \geq \beta$ Eq. S57 is unstable and non-linear terms have to be included. We also have $\eta'_P = \eta_P + b_P\eta_{mP}$, $\theta'_P = \theta_P + b_P\theta_{mP}$, and $W'_P = 2\beta P_{eq}(1 + b_P)/V$.

The autocorrelation of p can be calculated as

$$\begin{aligned} S_{p,p}(\tau) &= \int_{-\infty}^{+\infty} p(t+\tau)p(t)dt \\ &= F^{-1}\{\frac{W'_P}{\omega^2 + (\beta-\gamma)^2} + \frac{\theta'^2_P W_E}{[\omega^2 + (\beta-\gamma)^2](\omega^2 + \beta^2)}\} \\ &= \frac{W'_P}{2(\beta-\gamma)}e^{-(\beta-\gamma)|\tau|} - \frac{\theta'^2_P W_E}{2\gamma(2\beta+\gamma)}(\frac{e^{-\beta|\tau|}}{\beta} - \frac{e^{-(\beta-\gamma)|\tau|}}{\beta-\gamma}) \qquad \text{(S58)} \end{aligned}$$

Without extrinsic noise ($W_E = 0$), the normalized autocorrelation of p is

$$R_{p,p}(\tau)|_{W_E=0} = e^{-(\beta-\gamma)|\tau|}. \qquad \text{(S59)}$$

This autocorrelation has a sharp peak, whose FWHM is $\frac{2\log 2}{\beta-\gamma}$. With positive feedback, $\gamma > 0$, the peak is wider than no feedback. With negative feedback or auto-repression, $\gamma < 0$, the peak is narrower than no feedback. When P_{eq} is such that $Q(P)$ flattens out, γ is near zero, the feedback is inactive.

If the noise in P is dominated by extrinsic noise ($W'_P \ll W_E$),

$$R_{p,p}(\tau)|_{W'_P \ll W_E} \approx \frac{\beta(\gamma-\beta)}{\gamma}(\frac{e^{-\beta|\tau|}}{\beta} - \frac{e^{-(\beta-\gamma)|\tau|}}{\beta-\gamma}). \qquad \text{(S60)}$$

It has a rounded top as $\frac{d}{d\tau}R_{p,p}(\tau)|_{W'_P \ll W_E} \approx 0$. As usual the peak is wider when extrinsic noise dominates than when intrinsic noise dominates.

S3 Analytical solutions of microcolony approximation

It is usually assumed that the noise terms η_i in chemical kinetic equations have constant amplitudes, but this is only true, e.g., for a continuous stirred-tank reactor with fixed volume. In contrast, most cells double their volumes during the cell cycle. Moreover, at the level of a microcolony, the total volume change is so significant that it cannot be ignored.

As we have discussed, at steady state without other noise sources, a Poisson distribution is expected for molecules that are stochastically produced, diluted, and degraded. Hence within a fixed volume, the the standard deviation squared equals mean molecule number. As shown in Eqs. S26 and S29, W_i, the square of noise amplitude, is proportional to $\frac{1}{V}$:

$$W_{mA} = \frac{2\alpha_{mA}}{V}, \qquad W_A = \frac{2\alpha_A m_A}{V}, \tag{S61}$$

$$W_{mB} = \frac{2Q(A)}{V}, \qquad W_B = \frac{2\alpha_B m_B}{V}, \tag{S62}$$

$$W_{mP} = \frac{2Q(P)}{V}, \qquad W_P = \frac{2\alpha_P m_P}{V}. \tag{S63}$$

We assume $W_E \propto \frac{1}{V}$ as well.

We can then let $\eta_i = \eta_{i0} V^{-\frac{1}{2}}$, where η_{i0} is white noise with constant amplitude, independent of cell volume. With the dilution rate $\beta = \dot{V}/V$, the equations for fluctuations around equilibrium can be re-written in a volume independent way, if we let $x = x_0 V^{-\frac{1}{2}}$, where x is a concentration fluctuation ($x = \{m_a, a, m_b, b, m_p, p\}$). Considering Eqs. S11-S13 as example, they can be re-written as

$$\dot{E}_0 V^{-\frac{1}{2}} - \frac{1}{2} E_0 \dot{V} V^{-\frac{3}{2}} = -E_0 \dot{V} V^{-\frac{3}{2}} + \eta_{E0} V^{-\frac{1}{2}}, \tag{S64}$$

$$\dot{m}_{a0} V^{-\frac{1}{2}} - \frac{1}{2} m_{a0} \dot{V} V^{-\frac{3}{2}} = -\kappa m_{a0} V^{-\frac{1}{2}} + \eta_{mA0} V^{-\frac{1}{2}} + \theta_{mA} E_0 V^{-\frac{1}{2}}, \tag{S65}$$

$$\dot{a}_0 V^{-\frac{1}{2}} - \frac{1}{2} a_0 \dot{V} V^{-\frac{3}{2}} = \alpha_A m_{a0} V^{-\frac{1}{2}} - a_0 \dot{V} V^{-\frac{3}{2}} + \eta_{A0} V^{-\frac{1}{2}} + \theta_A E_0 V^{-\frac{1}{2}}. \tag{S66}$$

After canceling $V^{-\frac{1}{2}}$ from both sides of the equations and let $\beta_0 = \beta/2$, we found

$$\dot{E}_0 = -\beta_0 + \eta_{E0}, \tag{S67}$$

$$\dot{m}_{a0} = -(\kappa - \beta + \beta_0) m_{a0} + \eta_{mA0} + \theta_{mA} E_0, \tag{S68}$$

$$\dot{a}_0 = \alpha_A m_{a0} - \beta_0 a_0 + \eta_{A0} + \theta_a E_0. \tag{S69}$$

Comparing with Eqs. S11-S13, the effective protein synthesis rate α_A, and the mere degradation rate $\kappa - \beta$ are not changed, while the dilution rate β becomes β_0. Thus the form of the equations is preserved. All the correlation results derived with the constant volume assumption can still be used but with β replaced by $\beta_0 = \beta/2$. As a result, the correlation time scales are different at the single-cell level and at the microcolony level. For exam-

ple, without extrinsic noise or protein degradation, the autocorrelation peak width doubles at the microcolony level compared to at the single-cell level. The cross-correlation curve $R_{a,b}(\tau)|_{W_E=0}$ has an extreme value at $\tau = -0.72$ generation at the single-cell level. At the microcolony level, the extreme value is at $\tau = -1.44$ generations. Here, our calculations at the "single-cell level" ignore the volume change of cells during the cell cycle. Correlations at the single-cell level and at the microcolony level measured in experiments are compared in Fig. S2.

S4 Correlation as a tool to study non-steady state processes

Although correlation was defined above as a time-averaged quantity, with time course data of individuals in a population, we can calculate the correlation of cell-to-cell fluctuations at one time point (t_1) with those at another time point (t_2). With the time average no longer performed, the correlation can be used to study non-steady process. Take the simplified version of Eq. S8 as an example:

$$\frac{dA}{dt} = \alpha(t) - \beta(t)A + \eta(t), \tag{S70}$$

in which $\langle \eta(t) \rangle = 0$ and $\langle \eta(t_1)\eta(t_2) \rangle = W(t)\delta(t_1 - t_2)$. Let $a(t) = A(t) - \langle A(t) \rangle$, where $\langle A(t) \rangle$ is the population average of $A(t)$. We have

$$\frac{d\langle A(t) \rangle}{dt} = \alpha(t) - \beta(t)\langle A(t) \rangle, \tag{S71}$$

$$\frac{da(t)}{dt} = -\beta(t)a(t) + \eta(t). \tag{S72}$$

Let $\beta(t) = \frac{d\Psi(t)}{dt}$, Eq. S72 can be written as

$$\frac{d}{dt}[ae^{\Psi(t)}] = \eta e^{\Psi(t)}. \tag{S73}$$

$$a(t) = a(0)e^{\Psi(0)-\Psi(t)} + e^{-\Psi(t)} \int_0^t \eta(t')e^{\Psi(t')}dt'. \tag{S74}$$

The correlation is then

$$\begin{aligned}\langle a(t_1)a(t_2)\rangle &= a^2(0)e^{2\Psi(0)-\Psi(t_1)-\Psi(t_2)} + \\ &\quad a(0)e^{\Psi(0)-\Psi(t_1)-\Psi(t_2)}[\int_0^{t_1}\langle\eta(t')\rangle e^{\Psi(t')}dt' + \int_0^{t_2}\langle\eta(t'')\rangle e^{\Psi(t'')}dt''] \\ &\quad + e^{-\Psi(t_1)-\Psi(t_2)}\int_0^{t_1}\int_0^{t_2}\langle\eta(t')\eta(t'')\rangle e^{\Psi(t')+\Psi(t'')}dt'dt'' \\ &= a^2(0)e^{2\Psi(0)-\Psi(t_1)-\Psi(t_2)} + e^{-\Psi(t_1)-\Psi(t_2)}\int_0^{\min([t_1,t_2])} W(t')e^{2\Psi(t')}dt' \quad \text{(S75)}\end{aligned}$$

which helps to estimate how the correlation matrix responds to changes of cell state. Usually the protein dilution rate β is constant and $\Psi(t) = \beta t$. If the cell state changes at $t = 0$, the correlation matrix $\langle a(t_1)a(t_2)\rangle$ loses its memory of the initial state $a^2(0)$ via the decay of memory $e^{-\beta(t_1+t_2)}$. An example was simulated and is showed in Fig. S3.

In this study for the weak interaction between YFP-LuxO and mCherry-LuxR one can notice the slight difference when the cells were moved from liquid culture to under agarose pad (Fig. 4 *A*), suggesting the weak regulation was affected by the external environment. However, for the strong regulatory link between mCherry-LuxR and *qrr*4-*cfp*, the correlation was consistent over the course of observation (Fig. 2 *A*).

S5 Simulation of cross- and autocorrelations

We used Monte-Carlo simulations to investigate protein cross- and autocorrelation functions for a limited number of cells, and show how these correlations resemble the analytical solutions given in Sec. S2 and Sec. S3.

One can measure protein level fluctuations in a simulation and calculate the correlation functions. Under ideal conditions, the result would match the analytical solution when the number of cells and the observation time are infinite. In practice both are limited. To gain insight into how experimental results resemble analytical solutions, a Monte-Carlo simulation was performed using the Gillespie method (14).

As discussed in Sec. S2, protein A positively regulates B, while P represses its own production. In the simulation, the mean cell volume is 1 at the beginning of cell cycle. The protein concentration unit is copy number per unit volume. The time unit is the mean cell doubling time (generation). Taking into account the average volume of *V. harveyi* cells, which are about 2 μm long and 1 μm across, 1 molecule per cell corresponds to $\sim$2 nM.

For simplicity, extrinsic noise was not included in the simulation. We simulated

$$\frac{dA}{dt} = \alpha_A - \beta A \tag{S76}$$

$$\frac{dB}{dt} = \alpha_B \frac{A^h}{A^h + K^h} - \beta B \tag{S77}$$

$$\frac{dP}{dt} = \alpha_P \frac{K^h}{P^h + K^h} + \alpha_{P1} - \beta P \tag{S78}$$

The parameters are $\beta = \log 2$ (generation)$^{-1}$, $\alpha_A = 50\beta$, $\alpha_B = \alpha_P = 200\beta$, $\alpha_{P1} = 0$, $h = 2$, and $K = 50$ for active regulations. The sample time-traces are the blue and magenta curves in Fig. S1 *b* for A and B and the orange curve in Fig. S1 *f* for P. Two inactive auto-repression cases were also simulated for P. For the blue region in Fig. S1 *e*, $K = 1$, $\alpha_P = 200\beta$, and $\alpha_{P1} = 20\beta$. The sample time-trace is the blue curve in Fig. S1 *f*. For the white region in Fig. S1 *e*, $K = 1000$, $\alpha_P = 100\beta$, $\alpha_{P1} = 0$. The sample time-trace is the black curve in Fig. S1 *f*.

To make the simulations comparable to the experiments, every simulation examined $N = 100$ cells at time zero and each simulation spans 4 to 10 generations. To generate the initial cells, first a seed cell was simulated to grow and divide for 10 generations. At certain time point of the last generation, N of these 2^9 cells were picked at random for further simulation. Cell growth rate was set a constant and cell cycle-time has a Gaussian distribution centered at 1 with a standard deviation of 0.2. Correlation matrixes were calculated both at the single-cell level and at the microcolony level. The single-cell level correlation calculation follows (9).

In the experiment, the average protein concentration changed gradually over the 8-hour duration of the movie, possibly due to adaptation from the liquid culture to the immobilized state. The timescale of this gradual relaxation is several cell generations. As our interest is in gene regulation of timescale $\sim$1 cell generation, we filter out these slow variations, in a similar strategy to one used previously (15).

Experimental and simulation correlation matrixes are calculated according to Eq. S1 to S3. The correlation matrixes for simulated results are shown in Fig. S1 *c* for $R_{a,b}(t_A, t_B)$ and Fig. S1 *g* for $R_{p,p}(t_{P1}, t_{P2})$. As the regulatory links are invariant over time, the matrixes show similar values along the main diagonals. However, due to the small sample size and stochasticity of each time trace, the heat-maps of matrixes are not perfectly smooth. Such roughness matches the experimental results. To further summarize the correlation results, correlation curves which plot mean correlation values for $t_1 - t_2 = \tau$ is generated. Different correlation curves are shown in Fig. S1 *d* for $R_{a,b}(\tau)$ and *h* for $R_{p,p}(\tau)$ with black curves representing the theoretical values and colored curves for simulation results. Within the error bars, the simulated curves agree well with the theoretical values. The simulations suggest that at low protein levels when fluctuation amplitudes are larger than detection noise, cross- and autocorrelation are good tools to understand regulation between proteins under experimental conditions.

Comparison between correlations at the single-cell level and at the microcolony level

are shown in Fig. S2 *c* and *f*. Although the calculated results at the two levels differ significantly, they both agree with their respective analytical solutions.

A system that is at non-steady state was also simulated (Fig. S3). Initially protein A positively regulates protein B. After $t = 1$ generation, the regulation is removed and the equilibrium value is also changed for B. Before $t = 1$ generation,

$$\dot{A} = \alpha - \beta A, \tag{S79}$$

$$\dot{B} = 4\alpha \frac{A^h}{A^h + K^h} - \beta B. \tag{S80}$$

After $t = 1$ generation, the dynamics for A remains unchanged, but

$$\dot{B} = 1.5\alpha - \beta B. \tag{S81}$$

Here $\beta = \log 2$ generation^{-1}, $\alpha = 50\beta$, $K = 50$, $h = 2$. The cross-correlation matrix $R_{a,b}$ shows an asymmetrical pattern typical of A positively regulating B before $t = 1$. One generation after the change applies, $R_{a,b}$ becomes flat and near zero, as expected for two independent proteins with no extrinsic noise.

References

1. Bassler, B. L., E. P. Greenberg, and A. M. Stevens, 1997. Cross-species induction of luminescence in the quorum-sensing bacterium *Vibrio harveyi*. *J. Bacteriol.* 179:4043–4045.

2. Datsenko, K. A., and B. L. Wanner, 2000. One-step inactivation of chromosomal genes in *Escherichia coli* K-12 using PCR products. *Proc. Natl. Acad. Sci. U.S.A.* 97:6640–6645.

3. Bassler, B. L., M. Wright, R. E. Showalter, and M. R. Silverman, 1993. Intercellular signalling in *Vibrio harveyi*: sequence and function of genes regulating expression of luminescence. *Mol. Microbiol.* 9:773–786.

4. Long, T., K. C. Tu, Y. Wang, P. Mehta, N. P. Ong, B. L. Bassler, and N. S. Wingreen, 2009. Quantifying the integration of quorum-sensing signals with single-cell resolution. *PLoS Biol.* 7:e68.

5. Wang, L., W. C. Jackson, P. A. Steinbach, and R. Y. Tsien, 2004. Evolution of new nonantibody proteins via iterative somatic hypermutation. *Proc. Natl. Acad. Sci. U.S.A.* 101:16745–16749.

6. Teng, S. W., Y. Wang, K. C. Tu, T. Long, P. Mehta, N. S. Wingreen, B. L. Bassler, and N. P. Ong, 2010. Measurement of the copy number of the master quorum-sensing regulator of a bacterial cell. *Biophys. J.* 98:2024–2031.

7. Mount, D. W., 1980. The genetics of protein degradation in bacteria. *Annu. Rev. Genet.* 14:279–319.

8. Andersen, J. B., C. Sternberg, L. K. Poulsen, S. P. Bjorn, M. Givskov, and S. Molin, 1998. New unstable variants of green fluorescent protein for studies of transient gene expression in bacteria. *Appl. Environ. Microbiol.* 64:2240–2246.

9. Dunlop, M. J., R. S. Cox, J. H. Levine, R. M. Murray, and M. B. Elowitz, 2008. Regulatory activity revealed by dynamic correlations in gene expression noise. *Nat. Genet.* 40:1493–1498.

10. Svenningsen, S. L., C. M. Waters, and B. L. Bassler, 2008. A negative feedback loop involving small RNAs accelerates *Vibrio cholerae*'s transition out of quorum-sensing mode. *Genes Dev.* 22:226–238.

11. Tu, K. C., T. Long, S. L. Svenningsen, N. S. Wingreen, and B. L. Bassler, 2010. Negative feedback loops involving small regulatory RNAs precisely control the *Vibrio harveyi* quorum-sensing response. *Mol. Cell* 37:567–579.

12. Thattai, M., and A. van Oudenaarden, 2001. Intrinsic noise in gene regulatory networks. *Proc. Natl. Acad. Sci. U.S.A.* 98:8614–8619.

13. Cai, L., N. Friedman, and X. S. Xie, 2006. Stochastic protein expression in individual cells at the single molecule level. *Nature* 440:358–362.

14. Gillespie, D. T., 1996. Exact numerical simulation of the Ornstein-Uhlenbeck process and its integral. *Phys. Rev. E* 54:2084–2091.

15. Sigal, A., R. Milo, A. Cohen, N. Geva-Zatorsky, Y. Klein, Y. Liron, N. Rosenfeld, T. Danon, N. Perzov, and U. Alon, 2006. Variability and memory of protein levels in human cells. *Nature* 444:643–646.

Figure Legends

Figure S1.

Model and simulations of gene regulatory circuits and the correlation matrix of fluctuations.

(*a*) For a gene regulation network in which protein A positively regulates protein B, the steady-state concentration relation is shown as a sigmoidal curve. The static concentration [A] determines static [B]. Regions in which changes in [A] cause changes in [B] are labeled "Active" (*pink area*). When [A] falls outside of the active region, either too high or too low, the regulatory link from A to B is "inactive".

(*b*) Simulated time traces of protein A (*blue*) positively regulating protein B (*magenta*) in the active regime.

(*c*) Heat map of the correlation matrix $R_{a,b}(t_A, t_B)$ calculated at the single-cell level for the concentration fluctuations of proteins A and B (Eq. S3). The axes t_A and t_B define the times when fluctuations in protein concentrations A and B, respectively, are sampled. The value of the matrix element at (t_A, t_B) is indicated by the color. The contour lines tend to run parallel to the rising diagonal $t_A = t_B$. Higher values above the rising diagonal represent a positive regulatory link from A to B.

(*d*) The correlation curve (*blue*) plots the value of $R_{a,b}(t_A - t_B)$ versus $t_A - t_B$. The black curve plots the analytic solution of the linearized model (see Sec. S2).

(*e*) Plot of the production rate of a protein P repressing itself (*solid sigmoidal curve*). In the absence of auto-repression, the production rate is independent of [P] (*dashed line*). The protein degradation-dilution rate is directly proportional to the protein concentration (shown as a solid line passing through the origin). The static state is where the degradation-dilution rate line intersects the sigmoidal curve. Depending on where the degradation-dilution rate cross the production curve, there is no repression (*white*), active repression (*orange*), or saturated repression (*blue*).

(*f*) Simulated protein concentration versus t, without repression (*upper, black trace*), with active repression (*middle, orange trace*) and with saturated repression (*lower, blue trace*). The protein levels for both active and saturated repression are lower than without repression. However, with active repression, the protein level fluctuates faster than without repression or with saturated repression (the time scales for the final two are the dilution-degradation rate of the protein).

(*g*) Heat map of the autocorrelation matrix $R_{p,p}(t_{P1}, t_{P2})$, calculated at the single-cell level, of P fluctuation with active auto-repression.

(*h*) The autocorrelation curves (mean correlation value $R_{p,p}(t_{P1} - t_{P2})$ versus $\Delta t = t_{P1} - t_{P2}$) of several types of proteins: a stable protein with noisy production, such as protein A (*blue*), a stable protein regulated by another stable protein, such as protein B (*magenta*), an active auto-repressing protein, such as protein P with active auto-repression (*orange*). These autocorrelation curves mainly differ in peak widths. The black curves are the analytical solutions for the autocorrelation curves.

Figure S2.

Comparison between cross-correlation and autocorrelation curves obtained at the microcolony level and the single-cell level using the same data set. Correlations at the single-cell level or the microcolony level are different, but they each have well defined analytical solutions.

(*a, b*) The cross-correlation curves $R_{\mathrm{mCherry,CFP}}$ at the microcolony level (*a*) and at the single-cell level (*b*) at 0 nM AI (*blue*) and 50 nM AI (*green*). (*c*) Simulation results for protein A positively regulating protein B at the microcolony level (*orange*) and at the single-cell level (*pink*). Theoretical predictions are in gray. (*d, e*) Autocorrelation curves at the microcolony level (*d*) and at the single-cell level (*e*) for YFP-LuxO in the wt strain (*green*) and in the *luxO*-ar strain (*black*). All curves shown are at 0 nM AI. The solid gray line in (*d*) is $R(\Delta t) = e^{-\beta_0|\Delta t|}$, in (*e*) is $R(\Delta t) = e^{-\beta|\Delta t|}$, $\beta_0 = \beta/2$, $\beta = \log 2$ generation^{-1}. The experimental autocorrelation peak is wider than the theoretical prediction at the single-cell level, possibly due to partition noise at cell division. (*c*) Simulation results for a unregulated protein A at the microcolony level (*orange*) and at the single-cell level (*pink*). Theoretical predictions are in gray.

(*g, h*) Autocorrelation curves at the microcolony level (*g*) and at the single-cell level (*h*) for *qrr4-cfp* (*blue*) and mCherry-LuxR (*red*). All curves shown are at 0 nM AI. The solid gray lines are the same as those in (*d*) and (*e*). The dashed gray lines in (*g*) is $R(\Delta t) = e^{-\beta_0|\Delta t|}(1 + \beta_0|\Delta t|)$, and in (*h*) is $R(\Delta t) = e^{-\beta|\Delta t|}(1 + \beta|\Delta t|)$.

Correlations at the microcolony level and at the single-cell level were derived using the same batch of cells (30 to 40 microcolonies, 320 to 760 single-cell lineages).

Figure S3.

Simulation of a non-steady system.

(*a*) Simulation of protein A (*blue*) and protein B (*green*) concentrations in cells. Initially protein A positively regulates protein B. After $t = 1$ generation, the regulation is removed such that the equilibrium value is changed for B.

(*b*) Normalized cross-correlation $R_{a,b}$ between A and B concentration fluctuations. Before $t = 1$ generation (*lower dashed square*), $R_{a,b}$ showed an unsymmetrical pattern typical for A positively regulating B. After $t = 2$ (*upper dashed square*) $R_{a,b}$ is mostly zero and flat. The memory of previous regulation is rapidly lost.

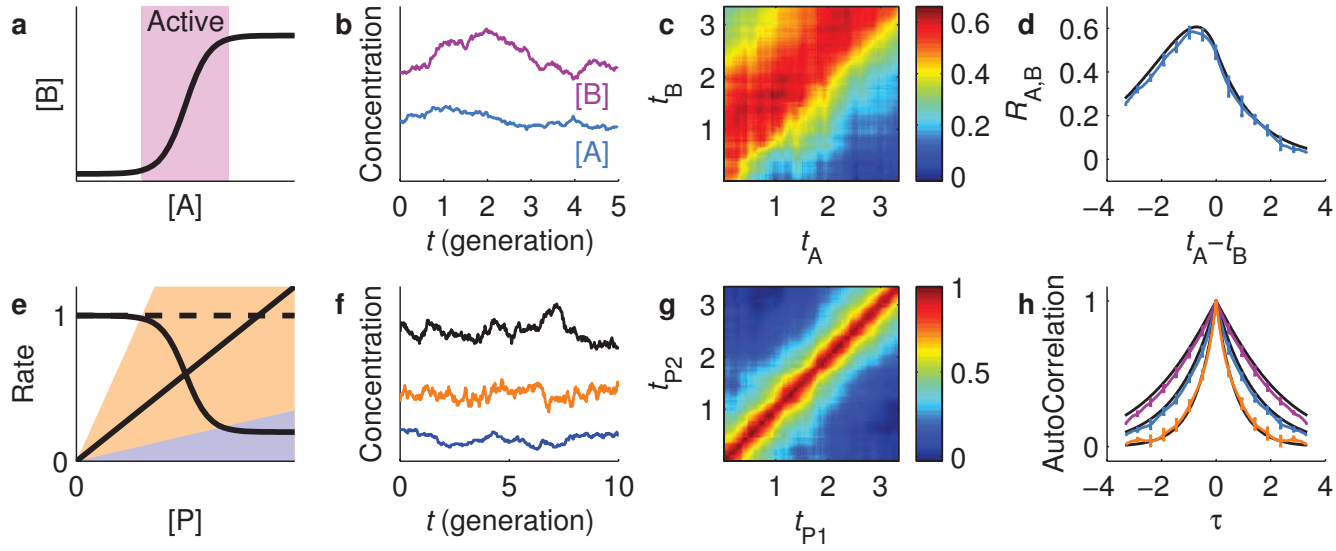
a
Active
[B]
[A]
b
Concentration
[B]
[A]
t (generation)
c
t_B
t_A
d
R_A,B
t_A−t_B
e
Rate
[P]
f
Concentration
t (generation)
g
t_P2
t_P1
h
AutoCorrelation
τ

Figure S1:

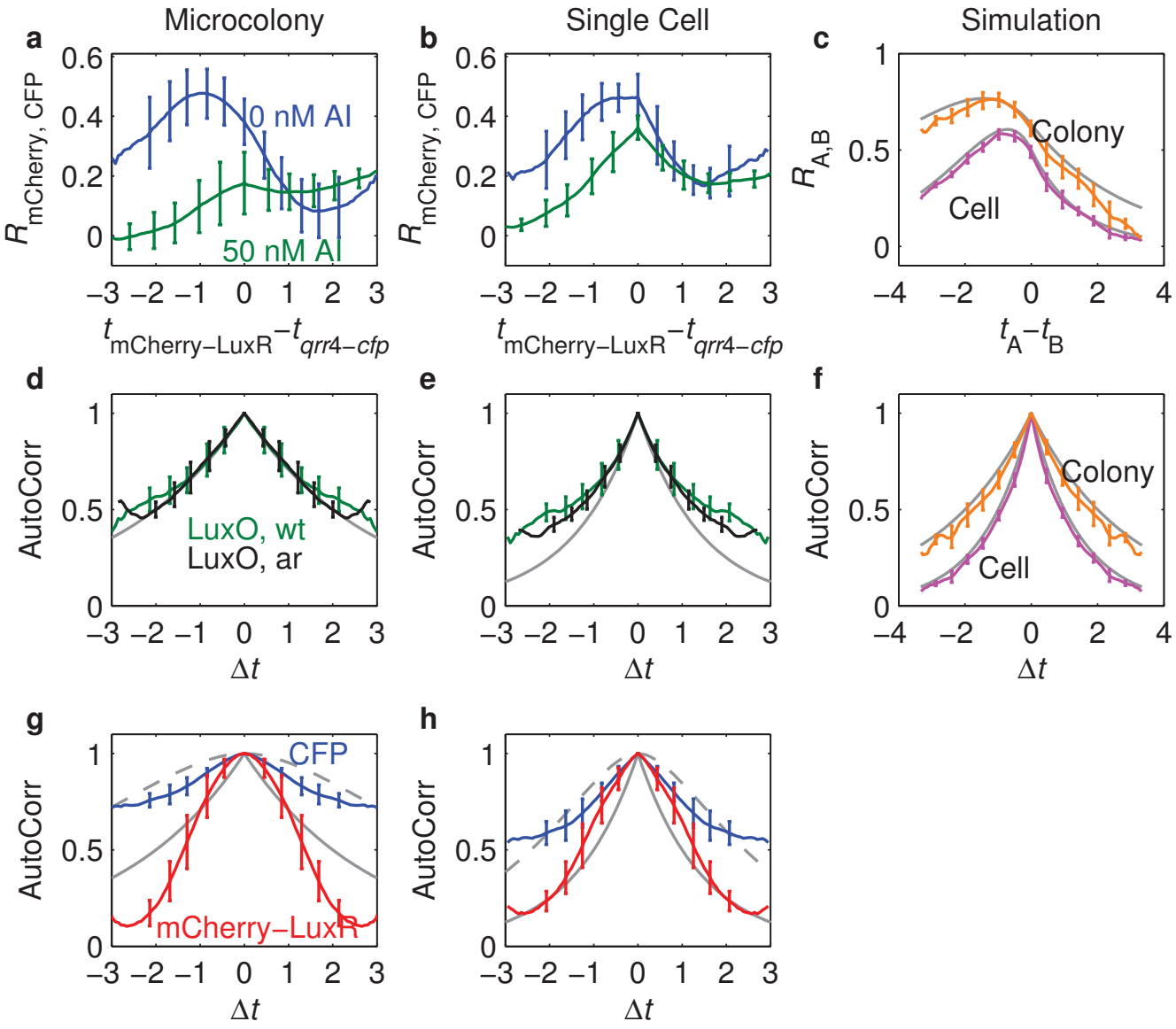
Microcolony
Single Cell
Simulation
a
b
c
d
e
f
g
h
$R_{\mathrm{mCherry,\ CFP}}$
$R_{\mathrm{A,B}}$
0 nM AI
50 nM AI
$t_{\mathrm{mCherry-LuxR}} - t_{qrr4-cfp}$
$t_{\mathrm{A}} - t_{\mathrm{B}}$
Colony
Cell
AutoCorr
LuxO, wt
LuxO, ar
CFP
mCherry–LuxR
Δt

Figure S2:

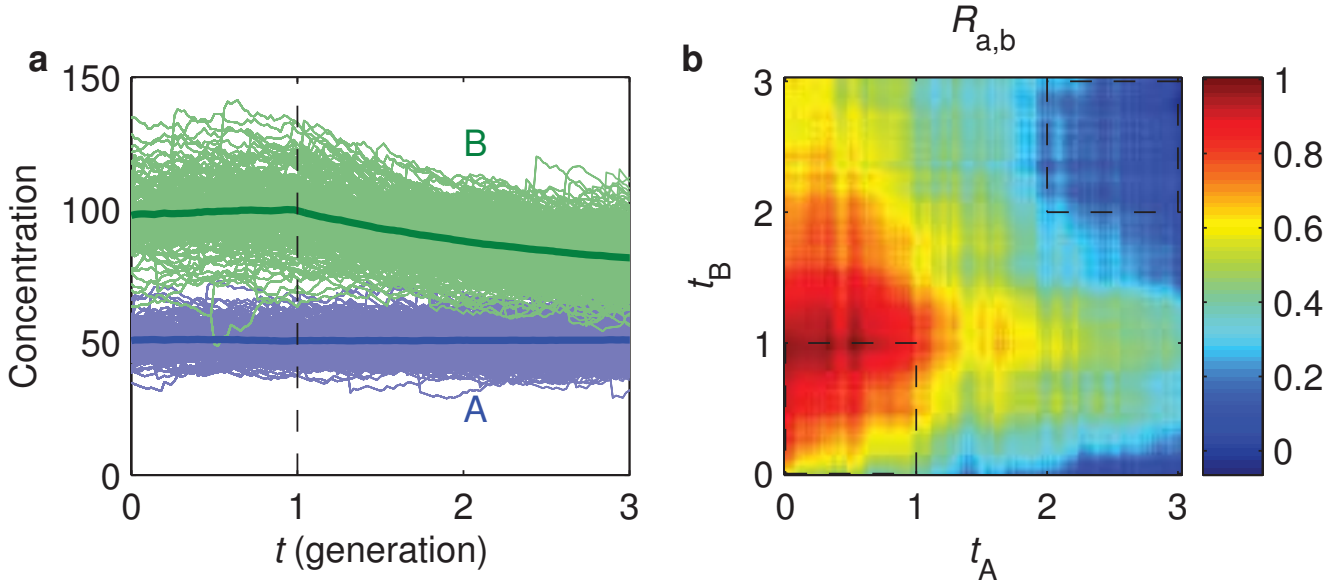
a
150
100
50
0
Concentration
B
A
0
1
2
3
t (generation)
b
R a,b
3
2
1
0
t B
0
1
2
3
t A
1
0.8
0.6
0.4
0.2
0

Figure S3: